Spectral Demand Curves Based on the Selected Strong Motion Records in Iran

Mehdi Zaré

Seismology Research Center, International Institute of Earthquake Engineering and Seismology (IIEES), Tehran, Iran, email: mzare@iiees.ac.ir

ABSTRACT: *Iranian strong motion data are studied to find the spectral demand ordinates of the selected records having better signal to noise ratios. The capacity spectrum method is used in this study and the spectral demand curves are estimated for 89 records. The records having low signal to noise ratio in the frequency range of less than 0.3Hz are excluded, and the rest of records with appropriate quality in long periods and a PGA (at least for one of the three-components) greater than 50cm/sec^2 are processed and analyzed. The site classification for these records is performed based on the receiver function method (estimating H/V ratio for any recorded motion). According to this procedure, the number of selected records were 22, 16, 25 and 26 for the site classes 1, 2, 3 and 4, respectively. The frequency contents of most records show dominant amplitudes between frequencies 0.2 and 10Hz. This selected catalog of 89 accelerograms is obtained from 45 earthquakes. The demand curves for these records are classified for horizontal and vertical components and for two major seismotectonic regions of Iran, Alborz-Central Iran and Zagros. The demand curves for 2 near-fault recorded motions in Bam and Tabas are classified separately while the average demand curves for such conditions are presented as well. These curves show significant difference between near and far fault motions as well as between rock and soft soil sites. However, no significant difference is distinguished between hard alluvium and deep incoherent soil classes which could be due to fewer available data for some site classes and unequal available data for different conditions.*

Keywords: Spectral; Demand curves; Strong motion; Noise ratios

1. Introduction

Spectral contents of the selected Iranian strong motion data are investigated in order to distinguish the demand curves for different categories of site classes and seismotectonic regions of Iranian plateau. The spectral demand curves are developed for Iran in this study to be used in Iranian projects of earthquake rehabilitation and reinforcement of important buildings started recently in the country. The records are selected in such a way that more than one accelerograms are recorded with higher qualities in lower frequencies and at least one component has a *PGA* greater than 50*cm/sec*^{2}. This study focuses on the records of higher quality and lower frequency noises.

Iranian National Strong Motion network comprises more than 1100 stations for which more than 3500 records have already been recorded (by March 2004). The records, obtained from the great events, are now available on website of Building and Housing Research Center (*BHRC*) [9] (an organization which maintains Iranian national strong motion network). The stations are selected all over the country; however, more than 30 stations are installed around Tehran. Meanwhile, according to higher seismicity of Zagros belt and population density in this region (south-west and western Iran), more stations are selected in Zagros. Therefore, most of the records are actually corresponded to Zagros belt [23].

Iranian National Strong Motion network has been initially installed by Kinemetrics, *SMA*-1 analog instruments (1975) and gradually expanded by *SSA*-2 digital instruments since Manjil earthquake of 1990; *Mw*7.3, in *NW* Iran. The records, studied in this paper, are mostly recorded digitally by *SSA*2 instruments. A corrected listing, based on Iranian strong motion which processed data until 1994, is presented in Bard et al [3]. The detailed parameters on such listing can be found in Zaré [24]. The site effect studies and site classification for Iranian strong motion stations are detailed in Zaré et al [22, 25].

In this paper, first, the procedure of data processing and records selection will be represented, and then, the strong motion parameters will be discussed. Finally, the obtained demand curves and the main results of the present study, are presented for each site classes and for the major seismotectonic regions of Iran.

2. Records Selection Criteria

Here, the records are selected based on their quality (evaluated according to their signal to noise ratio) and having at least one component with a peak ground acceleration greater than $50 cm/sec^2$. The total available data for the period of 1975-2003 were about 3100 three-components accelerograms.

The epicenters of 45 earthquakes are selected, for which 89 strong motion three-component accelerograms are recorded between 06 April 1977 and 26 December 2003. The source specifications for these earthquakes along with the details on the selected records, the coordinates of the epicenters and the strong motion stations are shown in Table (1). The stations are shown from class "1" to class "4". These site classes are assigned based on a detailed site effect study in Iran on the strong motion stations [25]. Figure (1) shows the distribution of data for each site class against the hypocentral distances. Most of the data are obtained from the stations located in the hypocentral distances of 8 to 100*km*.

This database is composed of fairly well known source parameters properly recorded. The moment magnitude and hypocentral distances for these records have thus been estimated directly from the strong motion records. The hypocentral distances were obtained from *S-P* time difference, while the seismic moment was directly calculated from the level of acceleration spectra plateau and the corner frequency [3, 8].

The magnitude range for the whole data set of records was *Mw*2.7 to 7.4, see Table (1). The distribution of magnitude against hypocentral distances, the range of which is 1-167*km*, is shown in Figure (2). The focal depth range for the events, relocated recently by Maggi et al [18], is 6 to 14*km*. The teleseismic information on focal depths are excluded from Table (1) [17], since such determination is very imprecise [3, 10, 19, 25]. The two horizontal components of any records are included separately in this study.

2.1. Filtering of the Accelerograms

In this study, the signal to noise ratio was considered to be significant only when the signal to noise ratio, R_{sn}, for both components exceeds a given threshold

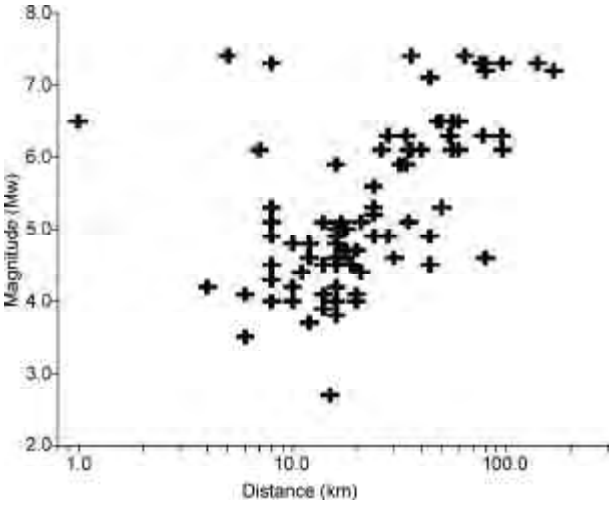

Figure 1. The site class against hypocentral distance for all of the data is presented in Table (1).

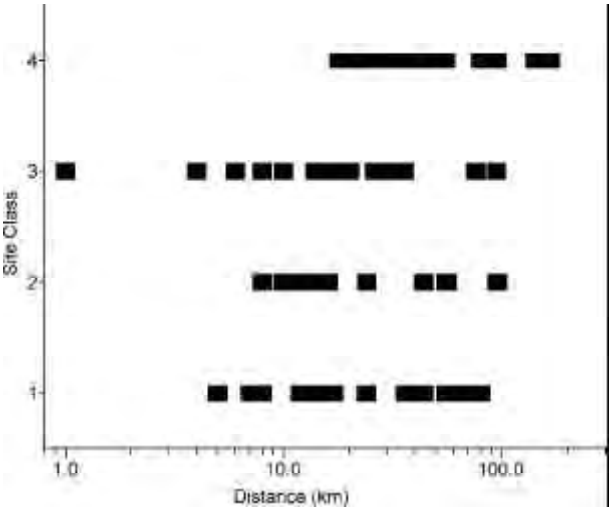

Figure 2. The magnitude-distance distribution for all stations on different site classes.

Table 1. Selected strong motion records for the present study.

No	Record	Station	Lat. N	Long. E	Site	BP Filter (Hz)	HPGA1 (Gal)	VPGA (Gal)	HPGA2 (Gal)	Earthquake	Mw	Foc. Mec	Hyp. Dist (km)
1	1054-01	Naghan	31.94N	50.74E	1	0.17-23.5	720	520	615	06/04/77	6.1	Rv	7
2	1082-01	Deyhuk	33.29N	57.50E	1	0.2-31	320	162	376	16/09/78	7.4	Rv	36
3	1083-01	Boshuyeh	33.86N	57.42E	1	0.27-17	98	87	94	16/09/78	7.4	Rv	64
4	1084-01	Tabas	33.60N	56.93E	1	0.1-40	1103	848	84	16/09/78	7.4	Rv	27
5	1139	Ghaen	33.72N	52.18E	1	0.1-39	197	119	134	27/11/79	7.1		44
6	1305	Kuhbanan	31.41N	56.29E	3	03-30	100	49	73	11/04/87	4.8		16
7	1300-01	Birjand	32.88N	59.21E	1	0.27-30	64	47	49	24/11/87	5.3		8
8	1353-01	Ghazvin	36.27N	50.01E	3	0.22-25	186	90	134	20/06/90	7.3	SS	76
9	1357-01	Lahijan	37.21N	50.33E	4	0.1-25	108	75	176	20/06/90	7.3	SS	96
10	1362-01	Abbar	36.92N	48.97E	1	0.1-25	526	548	503	20/06/90	7.3	SS	40
11	1364	Zanjan	36.66N	48.57E	1	0.1-25	125	51	60	20/06/90	7.3	SS	80
12	1372	Eshtehard	35.72N	50.36E	4	03-16	72	44	77	20/06/90	7.3	SS	140
13	1500-03	Zanjiran	29.10N	52.56E	2	0.25-39	72	27	61	14/03/94	4.3		8
14	1500-04	Zanjiran	29.10N	52.56E	2	0.2-39	64	36	75	17/03/94	4.8		12
15	1494-03	Kavar	29.21N	52.67E	2	0.2-39	52	39	47	17103/94	4.6		12
16	1500-05	Zanjiran	29.10N	52.56E	2	0.23-39	111	30	73	17103/94	4.2		16
17	1492-04	Zarrat	29.21N	52.77E	4	0.1-39	53	22	51	18/03/94	4.4		21
18	1500-08	Zanjiran	29.10N	52.56E	2	0.1-39	28	26	51	19/03/94	4.4		11
19	1492-05	Zarrat	29.21N	52.77E	4	0.1-39	37	20	51	23/03/94	4.7		20
20	1492-06	Zarrat	29.21N	52.77E	4	0.1-39	213	60	244	30/03/94	5.2		24
21	1492-08	Zarrat	29.21N	52.77E	4	0.1-39	57	21	49	03/04/94	5.2		24
22	1502-04	Zanjiran	29.10N	52.56E	2	0.1-39	193	73	180	05/06/94	4.8		10
23	1502-05	Zanjiran	29.10N	52.56E	2	0.1-39	38	19	71	06/06/94	4.2		10
24	1492-15	Zarrat	29.21N	52.77E	4	0.1-39	111	36	84	18/06/94	5.1		21
25	1502-08	Zanjiran	29.10N	52.56E	2	0.1-39	94	51	93	20/06/94	5.1		8
26	1492-16	Zarrat	29.21N	52.77E	4	0.2-40	318	112	280	20/06/94	5.9	SS	32
27	1493-02	Firouzabad	28.80N	52.57E	3	0.25-40	272	115	295	20/06/94	5.9	SS	34
28	1502-09	Zanjiran	29.10N	52.56E	2	0.2-40	1100	990	1090	20/06/94	5.9	SS	16
29	1501-01	Zanjiran	29.10N	52.56E	2	0.1-39	84	37	109	23/06/94	3.7		12
30	1501-07	Zanjiran	29.10N	52.56E	2	0.23-39	135	59	136	24/06/94	4.5		8
31	1523-23	Jovakan	29.05N	52.56E	1	03-39	70	30	66	19/09194	3.8		16
32	1528-01	Fin	27.65N	55.90E	3	03-39	54	33	32	28/10/94	4.2		4
33	1523-28	Jovakan	29.05N	52.56E	1	0.1-39	142	33	101	08/12/94	5		16
34	1519-04	Zarrat	29.21N	52.77E	4	0.1-39	65	23	54	15/12/94	4.7		20
35	1528-03	Fin	27.65N	55.90E	3	0.1-39	529	412	494	24/01/95	4.9		16
36	1528-22	Fin	27.65N	55.90E	3	0.1-39	53	27	42	24/01/95	4		16
37	1528-23	Fin	27.65N	55.90E	3	0.1-39	60	27	52	24/01/95	4		8
38	1528-26	Fin	27.65N	55.90E	3	0.1-39	179	83	143	24/01/95	4.5		16
39	1528-10	Fin	27.65N	55.90E	3	0.23-39	165	61	165	24/01/95	4.6		16
40	1528-12	Fin	27.65N	55.90E	3	0.23-39	84	51	84	24/01/95	4.1		6
41	1528-15	Fin	27.65N	55.90E	3	0.23-39	39	27	60	24/01/95	3.5		6
42	1528-17	Fin	27.65N	55.90E	3	0.23-39	54	21	35	24/01/95	3.9		14
43	1564-02	Khanzanu	29.70N	52.15E	1	0.1-39	52	24	56	23/10/95	4.9		8
44	1560-01	Lali	32.35N	49.09E	3	0.1-39	116	151	99	24/11/95	4.5		19
45	1560-04	Lali	32.35N	49.09E	3	0.1-39	78	81	105	27/11/95	5		18
46	1506-01	Hosseinieh	32.73N	48.25E	4	0.15-40	195	105	132	31/07/94	5.6	Rv	24
47	1549-04	Ammarloo	36.78N	49.76E	3	0.2-34	64	47	58	06/01/95	4		10
48	1547-01	Sefidrud	36.76N	49.38E	1	0.2-34	52	13	15	07/03/95	2.7		15
49	1620-01	Doab-Pol-Sefid	36.03N	53.02E	3	0.2-34	112	47	68	03/06/95	4		20
50	1626	Hassan-Keif	36.50N	51.40E	3	0.1-34	65	39	41	26/06/95	4.1		14
51	1620-01	Doab-Pol-Sefid	36.03N	53.02E	3	0.2-34	64	23	38	28/07/95	4.1		20
52	1571-10	Shabankarh	29.47N	50.98E	4	03-40	57	37	80	24/01/96	4.7	SS	18
53	1571-26	Shabankareh	29.47N	50.98E	4	0.23-39	23	27	81	25/01/96	4		20
54	1571-33	Shabankareh	29.47N	50.98E	4	0.3-20	170	90	70	26/01/96	4.6		80
55	1659-02	Ashkhaneh	37.61N	56.92E	4	0.2-25	118	35	102	04/02/97	6.5	SS	50
56	1707-02	Borezoo Dam	37.60N	57.97E	1	0.15-20	44	25	60	04/02/97	6.5	SS	60
57	1693-01	Ardebil-Ostandari	38.25N	48.30E	4	0.1-40	85	58	72	28/02/97	6.1	SS	36
58	1695-00	Astara	38.40N	48.85E	4	0.1-40	54	18	40	28/02/97	6.1	SS	40
59	1701-01	Ardebil-Maskan	38.24N	48.29E	4	0.08-40	122	64	130	28/02/97	6.1	SS	35
60	1702-00	Germi	39.03N	48.08E	3	0.2-20	52	21	48	28/02/97	6.1	SS	36
61	1716-00	Hir	38.60N	48.50E	2	0.15-30	59	20	34	28/02/97	6.1	SS	96
62	1724-00	Namin	38.40N	48.48E	2	0.15-40	72	34	106	28/02/97	6.1	SS	56
63	1725-00	Sarein	38.22N	48.08E	1	0.2-40	42	27	55	28/02/97	6.1	SS	60
64	1833-02	Karigh	37.87N	48.05E	3	0.25-40	578	197	672	28/02/97	6.1	SS	26
65	1920-04	Karigh	37.87N	48.05E	3	0.2-30	68	19	53	21/03/97	4.6		30
66	1921-01	Sarein	38.22N	48.08E	1	0.2-40	38	63	42	21/03/997	4.6		12
67	1927-03	Nir	38.08N	47.97E	3	0.2-40	127	48	125	21/03/97	4.6		16
68	1753-00	Sangan	34.38N	60.26E	1	0.08-40	118	82	112	10/05/97	7.2	SS	80
69	1758-00	Torbat-e-Heydarieh	35.25N	59.22E	4	0.08-20	40	18	52	10/05/97	7.2	SS	167
70	2161-00	Kerman-Farmandari	30.27N	57.11 E	4	0.3-20	31	22	58	18/11/98	5.3	SS	50
71	2176-01	Shahdad	30.39N	57.73E	1	0.2-20	52	38	48	18/11/98	5.3	S5	24
72	2373-01	Yekan	38.72N	48.42E	1	0.2-30	57	42	38	18/11/98	4.9		44
73	2322-00	Zanjireh	38.45N	45.35E	2	0.2-30	98	33	82	18/11/98	4.9		24
74	2369-01	Tasuj	38.30N	45.40E	4	0.3-40	59	27	56	18/11/98	4.9		28
75	2224-03	Derakht-e Toot	35.75N	61.10E	1	0.15-40	138	145	245	05/12/99	5.1	Rv	14
76	2225-11	Salehabad	35.70N	61.10E	1	0.2-40	138	142	102	05/12/99	5.1	Rv	17
77	2286-05	Nargeszar	29.45N	51.90E	2	0.15-40	143	87	195	05/12/99	4.5		14
78	2355-03	Baladeh	29.28N	51.93E	2	0.25-40	78	44	75	05/12/99	4.5		44
79	2465-01	Chehel-Zarei	29.46N	50.85E	4	0.2-35	65	33	76	03/05/00	5.1	R-SS	35
80	2748-01	Abegarm	35.74N	49.28E	4	0.11-28	130	55	125	22/06/02	6.3	Rv	34
81	2749-01	Avaj	35.58N	49.22E	3	0.10-25	465	250	445	22/06/02	6.3	Rv	28
82	2754-01	Kabodar-Ahang	35.20N	48.73E	1	0.20-40	78	71	155	22/06/02	6.3	Rv	78
83	2756-01	Rozon	35.39N	49.02E	4	0.18-40	182	132	200	22/06/02	6.3	Rv	55
84	2763	Abhar	36.15N	49.22E	4	0.18-20	32	27	73	22/06/02	6.3	Rv	55
85	2769	Darsachin	36.03N	49.23E	4	0.15-20	52	44	72	22/06/02	6.3	Rv	54
86	2778	Ghohrud	35.47N	48.07E	3	0.08-18	51	23	88	22/06/02	6.3	Rv	95
87	3162-1	Mohammad-Abad-e Maskun	29.97N	57.88E	4	0.1-40	120.1	69.2	71	26/12/03	6.5	SS	48
88	3168-2	Bam	29.12N	58.38E	3	0.11-40	992	775	623	26/12/03	6.5	SS	12
89	3176-1	Abaragh	29.38N	57.97E	1	0.1-40	162.6	83.2	107.7	26/12/03	6.5	SS	56

value of 3. The signal to noise ratio (R_{sn}) is computed, as estimated [22]:

$$(R_{sn}) = \frac{S(f)/\sqrt{t_1}}{N(f)/\sqrt{t_2}} \quad (1)$$

Where t_1 and t_2 are the window duration for the signal and noise parts, respectively. Since the records applied in this study are mostly recorded digitally, in most cases the time windows for noise parts (t_2) are selected before the p-unset (in the pre-event part of the records, mostly from 0 to 4 seconds, in the selected records). In analog records, (records until 1990), the noise windows are selected at the end part of the accelerogram where the amplitudes of the signals are minimized. A R_{sn} ratio over 3 is selected as the proper ratio to distinguish the signal from the noise. The data of low signal qualities, below 0.3*Hz*, are excluded in order to keep the records of acceptable low frequency contents. The high-pass and low-pass filters are hence selected for the parts with the signal to noise ratio over 3, and are shown in the column 7 of Table (1), (for both horizontal and vertical components, filter bands are found to be the same).

2.2. Magnitude Values

The moment magnitude is used here to give a uniform and reliable scale for comparing different parameters. The moment magnitude was systematically calculated for all selected records, i.e. well recorded earthquakes with little noise.

The source model, used to estimate the moment magnitude in this study, is based on Haskell [16] who proposed a simple source model for the estimation of high frequency ground motions. The simple seismic source models are explained by Aki [1] and Brune [7-8]. In this model, the far-field displacement spectrum is characterized by a flat level, $\overline{W}_0$, proportional to M_o at long periods, a corner frequency, *fc*, inverse proportional to the source dimension, and a high frequency spectral decay in the form $(f / fc)^{-\gamma}$. Taking γ values as 2 or 3, we have ω-square or ω-cube model, respectively (ω is the angular frequency in radians per second, equal to $2\pi f$). Hanks [12] has shown that with a ω-square model for which the acceleration spectra will be flat after the corner frequency, *fc*, the high frequency decay can be explained by the attenuation caused by the path effects. The more complicated and dynamic ω-cube model [7], shows that the rupture nucleation generates high frequency energy propor-tional to ω^{-3}. As proposed by Hanks and Kanamori [13], the displacement spectra may be represented as follows:

$$\overline{W} = \frac{\overline{W}_0}{1+\left(\frac{f}{f_c}\right)^{\gamma}} \quad (2)$$

If $\overline{W}_0$ is the value of the flat part of the displacement spectrum, the value of the flat part of the acceleration spectrum, A_0, may be related to $\overline{W}(0)$ with $A_0 = \overline{W}_0 \cdot \omega_c^2$ proportional to the seismic moment, M_o. For far-field S-waves, due to a double couple source embedded in an elastic, homogeneous, isotropic bounded medium [12], we have:

$$M_o = \frac{A_0}{(2\pi f_c)^2} \cdot \frac{4\pi R_h \cdot \rho \cdot \beta^3}{R'_{\theta\varphi} \cdot F_s} \quad (3)$$

Where β is the shear wave velocity of the medium, ρ is the density of elastic medium, around (2.8×10^3) kg/m^3, R_h is the hypocentral distance, $R'_{\theta\varphi}$ is the double couple radiation pattern for *SH* or *SV* waves (about 0.6 in average), F_s is the free space amplification factor (to be taken equal to 2) [4]. As shown below, to calculate M_o (in *N-m*), β is taken equal to 3500*m/sec* [16], $\rho = 2.8 \times 10^3 kg/m^3$.

Hanks and Kanamori [13] defined a new magnitude scale based on the seismic moment more reliable measure of the size of the great earthquakes. Taking into account the coefficients for *N-m* unit of M_o, this scale could be written as:

$$M_w = 0.667 \cdot \log M_o - 6.0 \quad (4)$$

Here, the Eqs. (3) and (4) have been used to calculate *Mw* for the events listed in Table (1).

2.3. Peak Ground Acceleration

After filtering the records (explained in 2.1), the values of peak ground acceleration (*PGA*) for different components are shown in columns 8 to 10 in Table (1). Most of the data are distributed over the hypocentral distances of 10 to 100 kilometers and the fmax values found for the vertical components, are systematically greater. However, still there is not enough data to develop the empirical relationship between *fc* and *fmax* values and *PGA*.

2.4. Site Classification

Site classes are estimated based on the transfer function method in which *H/V* amplification function is calculated to find the fundamental frequency of the site [25]. However, the site specific studies are performed for the sites studied in this paper, shown in Table (1), in view of the microtremor measurements and the seismic wave velocity profiling [25]. The formulation used for *H/V* method is based on the spectral ratio (R_{hv}) between the smoothed horizontal components and the smoothed vertical component:

$$R_{hv} = \frac{\sqrt{S_{H1}^2 / 2\sqrt{T_{H1}} + S_{H2}^2 / 2\sqrt{T_{H2}}}}{S_v(f) / \sqrt{T_V}} \quad (5)$$

Where T_{H1}, T_{H2} and T_V are the signal duration for the two horizontal components and one vertical one, respectively. Since the same time windows are used for all components, this formula might be simplified as:

$$R_{hv} = \frac{[1/2(S_{H1}(f) + S_{H2}(f))]}{S_v(f)} \quad (6)$$

Site class "1" is defined as the sites that do not exhibit any significant amplification below 15*Hz*. Site class 2 is determined as the sites for which the receiver function (*RF*) exhibits a fundamental peak exceeding 3 at a frequency located between 5 and 15*Hz*. Site class 3 is representative of the sites for which *RF* shows the peaks between 2 and 5*Hz*. Finally, site class 4 is defined as the sites for which *RF* indicates the peaks in frequencies below 2*Hz*, and it may be viewed as corresponding to thick soft alluvium.

H/V ratio is shown in Figure (3) for Bam strong motion station in order to indicate the stability of such assessment of fundamental frequency as for the site class. Figure (3a) indicates this ratio for Bam earthquake mainshock (26 December 2003, *Mw*6.5) and Figure (3b) represents *H/V* ratio for its 13 aftershocks. The figure indicates the stability of the amplification specially for the frequencies between 2 and 8*Hz*. According to Zaré et al [25], this site should be classified as class-3. Another study, Askari et al [2], indicates that the strong motion station of Bam was located in an area in Bam showed a shear wave velocity around 300 to 500*m/sec*. These results coincide with the calculated fundamental frequency for the site between 2 to 5*Hz*.

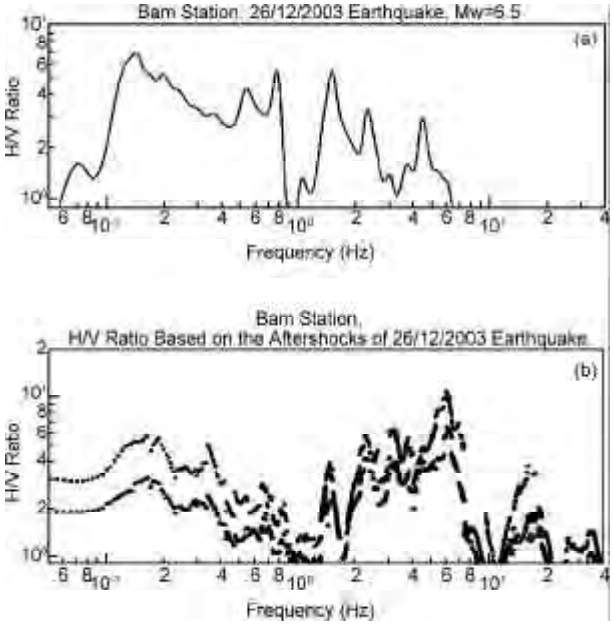

Figure 3. The PGA - hypocentral distance distribution for data recorded on site classes; a: '1'; b:'2'; c: '3'; and c: '4'. Crosses and circles stand for the horizontal components and the rectangulars show the vertical components.

This ranking was the result of the geotechnical measurements on 50 sites (compressional and shear wave velocity and microtremors) and the calculation of the receiver function for the strong motions using three component accelerograms. This categorization shows some similarities to that of Boore et al [5-6] (based on the average *Vs* for the 1^{st} 30*m*) for American northwestern data. The average *Vs* limits to distinguish the site classes in Boore et al [5-6] reports are 18*m/sec*, 360*m/sec*, 750*m/sec* and greater than 750*m/sec* (to be compared with our values of 300, 500 and 700*m/sec*).

2.5. Distance Variable

In discussing the choice of the "distance parameter", one must keep in mind the significant uncertainties in teleseismic epicenter localization and large uncertainties in determining focal depths for the Iranian earthquakes. It is important however, to define this parameter so that the future application of these data in establishing the attenuation laws will be easy.

In this study, it is decided to define the distance variable for the regression as the "hypocentral distance". This distance is controlled by the variations in the arrivals of the compressional and shear wave of each record. Such information is available without any ambiguity only with *SSA*-2 digital records

(herein, all studied records were obtained by such type of recorders).

In the case of major earthquakes, recorded in a near-fault distance, the surface distance to the fault is taken into account in place of the hypocentral distance, according to the source dimension in such earthquakes. Two records had such situations to be considered as the near-fault data; Tabas record of 16/09/1978: Tabas earthquake (*Mw*7.4) obtained in a 5*km* surface distance to the surface earthquake fault [24] and Bam record of 26/12/2003: Bam earthquake (*Mw*6.5) with a 1*km* surface distance to Bam surface earthquake fault rupture [26].

2.6. Fault Mechanism

According to the regional tectonic conditions of Iranian plateau, the fault mechanisms of most earthquakes are compressional, strike-slip or a combination of these two mechanisms. The fault mechanisms of most earthquakes used in the present study were strike-slip, compressional or a combination of these two mechanisms [15, 19]. The available information on focal mechanisms are presented in column 22, Table (1). In an earlier study [3, 24], it is shown that the focal mechanisms of the records for which the source parameters could be found comprising mostly strike-slip/reverse mechanisms, pure strike slip, pure reverse and pure vertical plane.

3. Capacity Spectrum Method and Spectral Demand Curves

Spectral demand curves are represented and discussed in the recent years to provide the input for the design methods using the energy dissipation in selected components of the framing system for maximum earthquake shaking [14, 21]. These curves are developed in this paper for the first time for Iranian selected strong motion records.

3.1. Methodology

This method is based on the assumption that the response of a building can be related to the response of an equivalent Single Degree of Freedom (*SDOF*) system. This implies that the response is controlled by a single mode while the shape of this mode remains constant throughout the response history. The consequence of the assumption is the reliable assessment of maximum seismic response of the Multi-Degree of Freedom Buildings (*MDOF*), such that the provided response is dominated by the first mode. The method applies the initial effective stiffness and secant stiffness information to calculate the target displacement. The methodology applies usually higher damping values based on the shape of the hysteresis and the maximum deformation level. Using this method, it is necessary to estimate the target displacement. Having the equivalent viscous damping, a design response spectrum for that damping could be developed. The acceleration response spectrum could be related to the displacement response spectrum by multiplying its ordinates by a factor of $T/4\pi^2$. By increasing the damping value, the acceleration and displacement spectral ordinate decrease. This relationship between the acceleration and displacement spectral ordinates shows that they can be related to each other in a simple plot, which is called the demand curve.

The spectral acceleration and displacement ordinates are plotted for different selected equivalent viscous damping values, in which the radial lines represent the constant period. This form of design loading can be directly compared with the non-linear load-deformation envelope with the response spectrum for the appropriate damping value, normalized with respect to the equivalent *SDOF* coordinates [11]. According to this method, the target displacement for the equivalent *SDOF* system is at the intersection of the load deformation envelope with the response spectrum for the appropriate damping level.

The response of a structure reduces with a damping system by the coefficient based on the effective damping of the interested mode. The reduction in the earthquake design response of the fundamental mode is due to the effective damping coefficient (B_{1D}). The capacity curve is a plot of the non-linear behavior of the fundamental mode in the plot of spectral acceleration against spectral displacement. Effective damping is a combination of three damping values [20]:

- Inherent damping (β_1), at or just below yield, which is typically assumed to be 5% of critical damping for the structures without dampers.
- Hysteretic damping (β_H), post yield hysteretic damping of the seismic-force-resisting-system at the amplitude of interest which is taken as 0% of critical at or just below the yield.
- Added viscous damping (β_V), viscous component of the damping systems which is taken as 0% for the hysteretic or friction-based damping systems.

3.2. Demand Curves for Iranian Strong Motions

Demand curves are developed for the selected records listed in Table (1). In order to provide a basis for comparing the spectra and easier use of these curves in the future, the spectral displacement (*Sd*) values are represented in *m/sec* and they are plotted against the spectral accelerations (*Sa*) normalized to the greatest peak acceleration (at the period of $T = 0.0$ second). The records are classified into two major Iranian seismotectonic zones of Alborz-Central Iran (where the strong motions are attenuated slower than Zagros, and are recorded with greater durations) and Zagros, showing faster attenuation and lower durations of strong motions [3, 24].

The classification of the records is extended to their site class [25] and the present study. Therefore, the demand curves and the displacement spectra are represented for such classes and also for the horizontal and vertical components. All of the spectral ordinates are developed for the damping values of 1, 3, 5, 7, and 10% of critical damping.

The demand curves are plotted for Bam accelerogram of the 26 December 2003 Bam earthquake (*Mw*6.5) in Figure (4). This motion is recorded in a surface distance of 1km to the earthquake fault trace [26]. According to the level of *PGA* in these two records (both with *PGAs* greater than 1*g*) and their close distance to the surface trace of the earthquake faults, the author has decided to analyze these two three-component records separately as the near-fault motions. The site studies for these two records show the site class '1' and '3' for Tabas and Bam stations, respectively.

3.3. Demand Curves for Different Seismotectonic Zones and Site Classes

The mean values of the demand curves (after normalization of Sa) are estimated and presented for horizontal and vertical components in Figures (5) to (8) for the site classes 1, 2, 3 and 4, respectively, based on the records in Alborz-Central Iran region. The demand curves estimated for two accelerograms recorded in Tabas and Bam (both recorded in Alborz-Central Iran zone) are separated from these data, and their mean spectra are presented for the "near-fault" conditions in Iran later in the paper. The mean demand curves for the record obtained in Zagros region are presented in Figures (9) to (12) for the site classes 1, 2, 3 and 4, respectively.

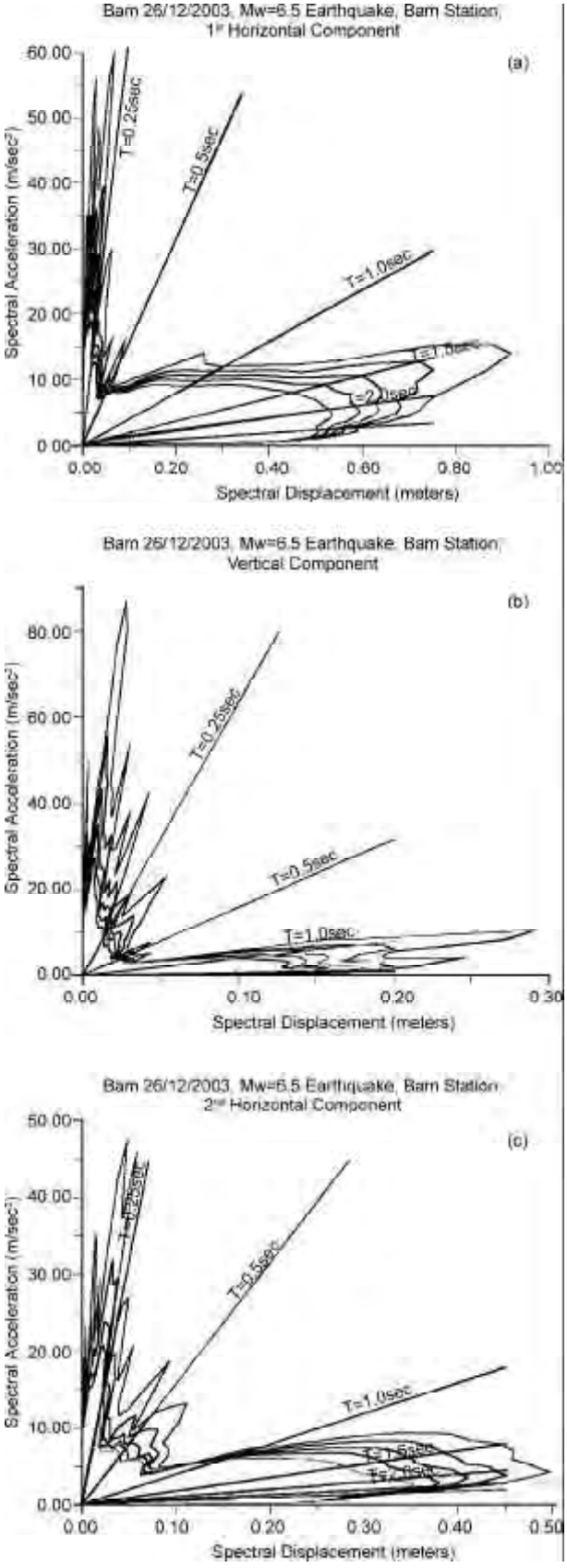

Figure 4. Demand curves of Bam record of 26/12/2003 Mw 6.5, for the a) 1st horizontal, b) vertical and c) 2nd horizontal component. The spectral ordinates are presented for different damping of 1, 3, 5, 7, and 10%, and the highest spectrum represent 1% damping and the lower spectra are for 3, 5, 7 and 10% of damping, respectively.

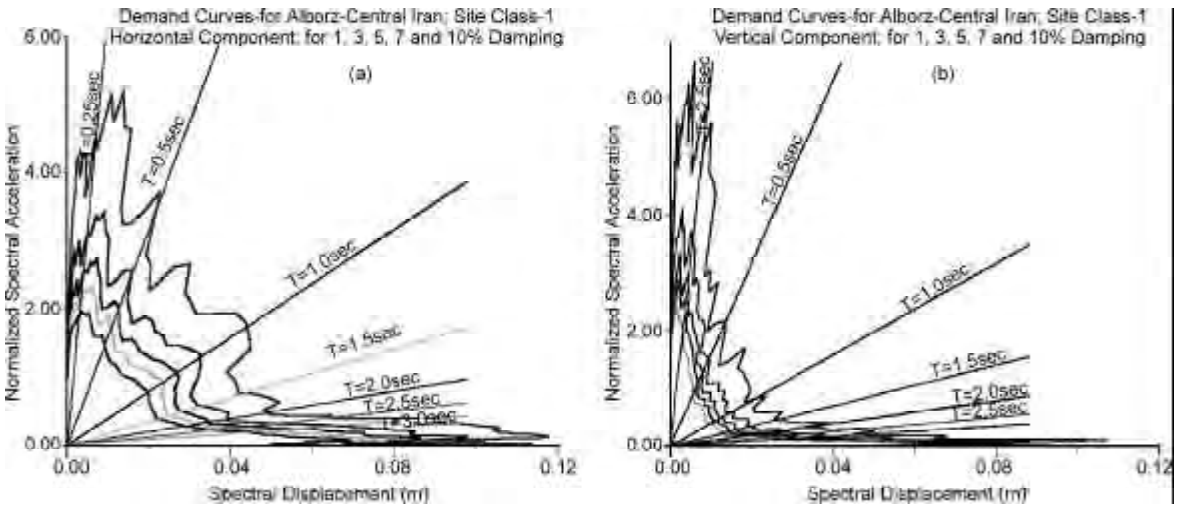

Figure 5. Mean demand curves of Alborz-Central zone, site class-1, for a) horizontal and b) vertical components. The spectral ordinates are represented for different damping of 1, 3, 5, 7, and 10%, and the highest spectrum represent 1% damping and the lower spectra for 3, 5, 7 and 10% damping, respectively.

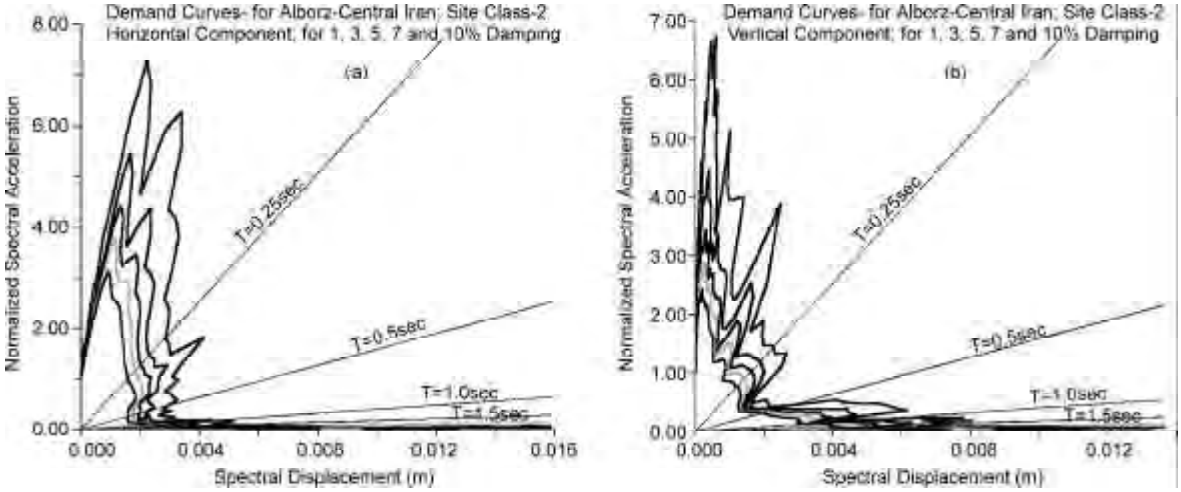

Figure 6. Mean demand curves of Alborz-Central zone, site class-2, for a) horizontal and b) vertical components. The spectral ordinates are represented for different damping of 1, 3, 5, 7, and 10%, and the highest spectrum represent 1% damping and the lower spectra are for 3, 5, 7 and 10% damping, respectively.

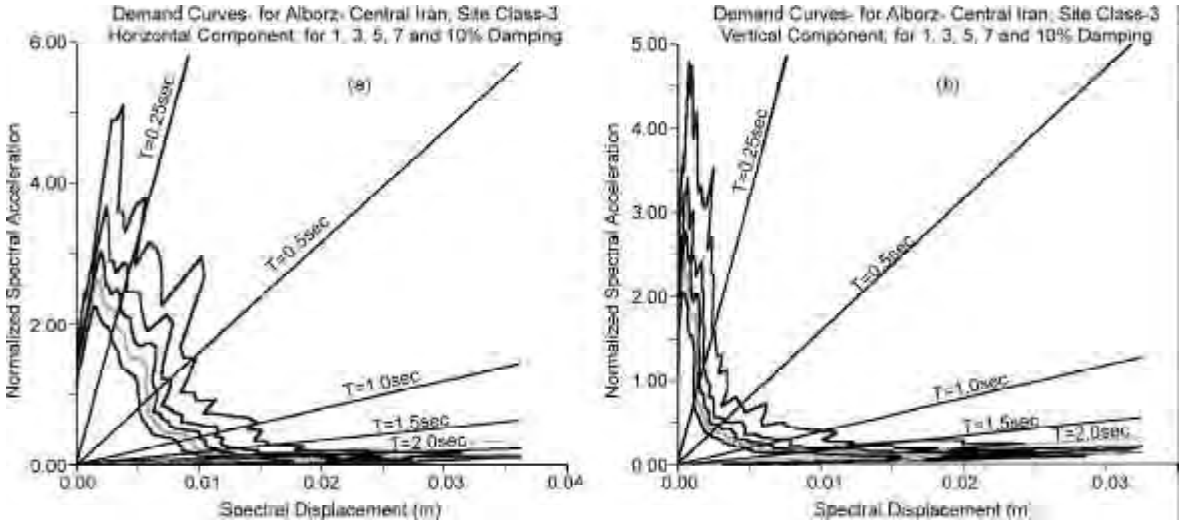

Figure 7. Mean demand curves of Alborz-Central zone, site class-3, for a) horizontal and b) vertical components. The spectral ordinates are represented for different damping of 1, 3, 5, 7, and 10%, and the highest spectrum represent 1% damping and the lower spectra are for 3, 5, 7 and 10% damping, respectively.

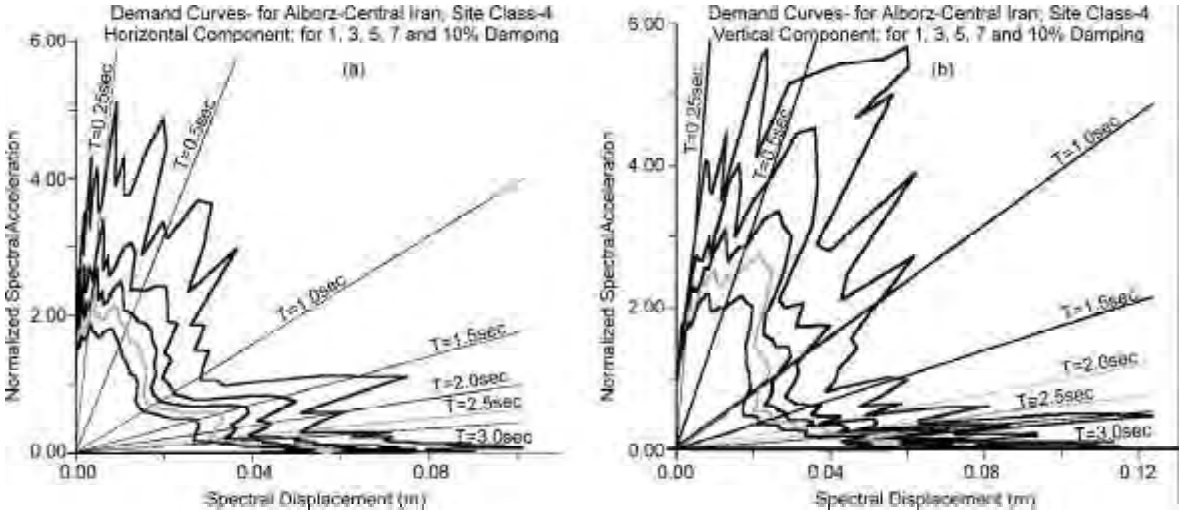

Figure 8. Mean demand curves of Alborz-Central zone, site class-4, for a) horizontal and b) vertical components. The spectral ordinates are represented for different damping of 1, 3, 5, 7, and 10%, and the highest spectrum represent 1% damping and the lower spectra are for 3, 5, 7 and 10% damping, respectively.

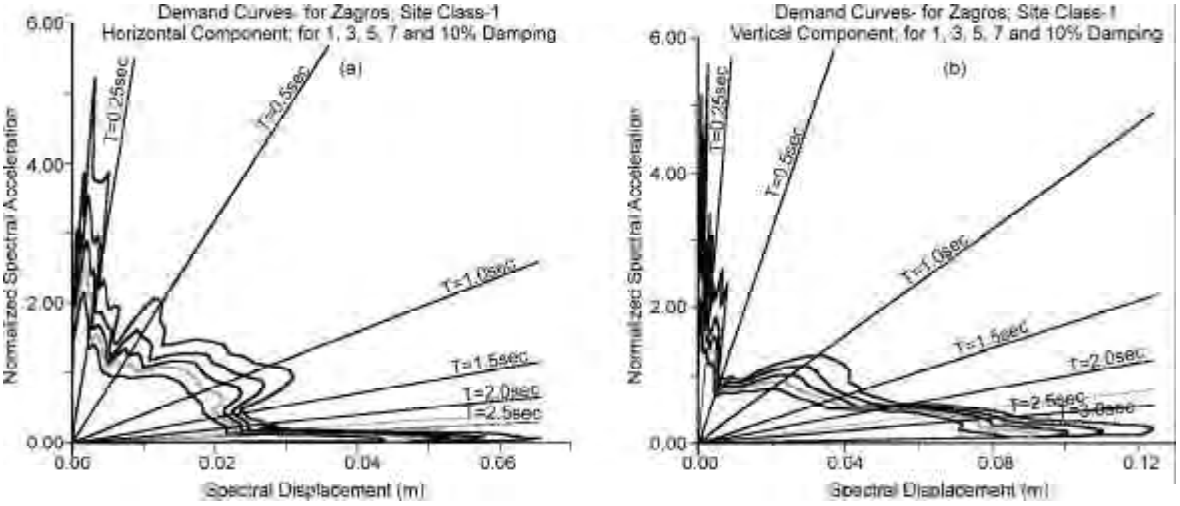

Figure 9. Mean demand curves of Zagros zone, site class-1, for a) horizontal and b) vertical components. The spectral ordinates are represented for different damping of 1, 3, 5, 7, and 10%, and the highest spectrum represent 1% damping and the lower spectra are for 3, 5, 7 and 10% damping, respectively.

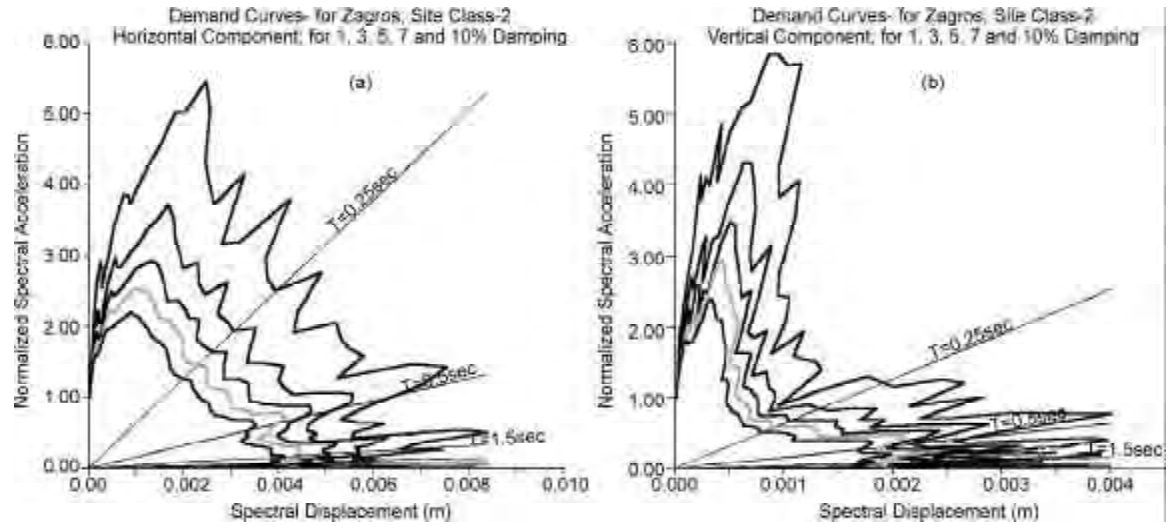

Figure 10. Mean demand curves of Zagros zone, site class-2, for a) horizontal and b) vertical components. The spectral ordinates are represented for different damping of 1, 3, 5, 7, and 10%, and the highest spectrum represent the 1% damping and the lower spectra are for 3, 5, 7 and 10% damping, respectively.

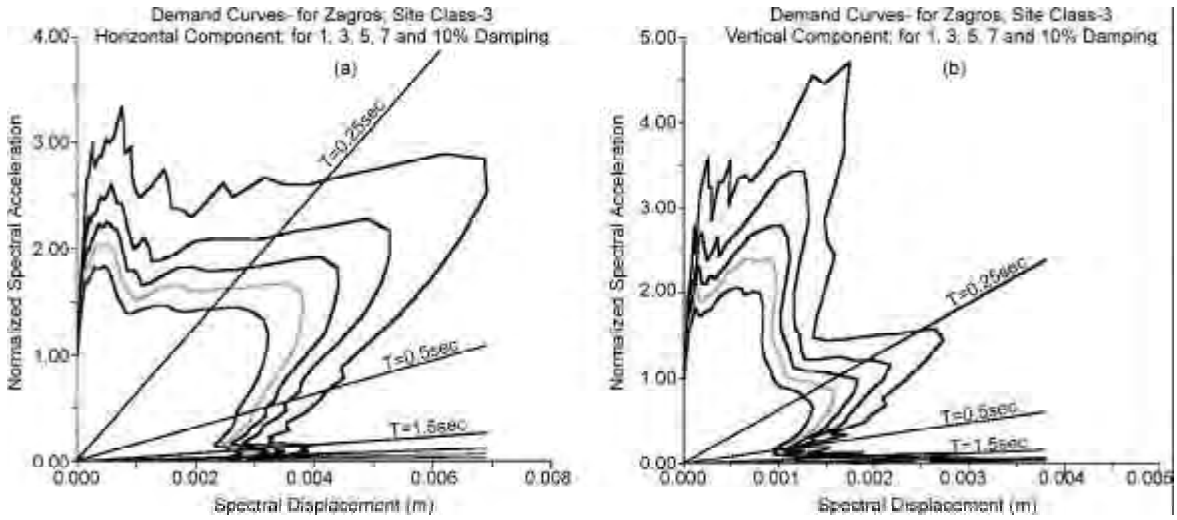

Figure 11. Mean demand curves of Zagros zone, site class-2, for a: horizontal and b: vertical components. The spectral ordinates are represented for different damping of 1, 3, 5, 7, and 10%, and the highest spectrum represent the 1% damping and the lower spectra are for 3, 5, 7 and 10% damping, respectively.

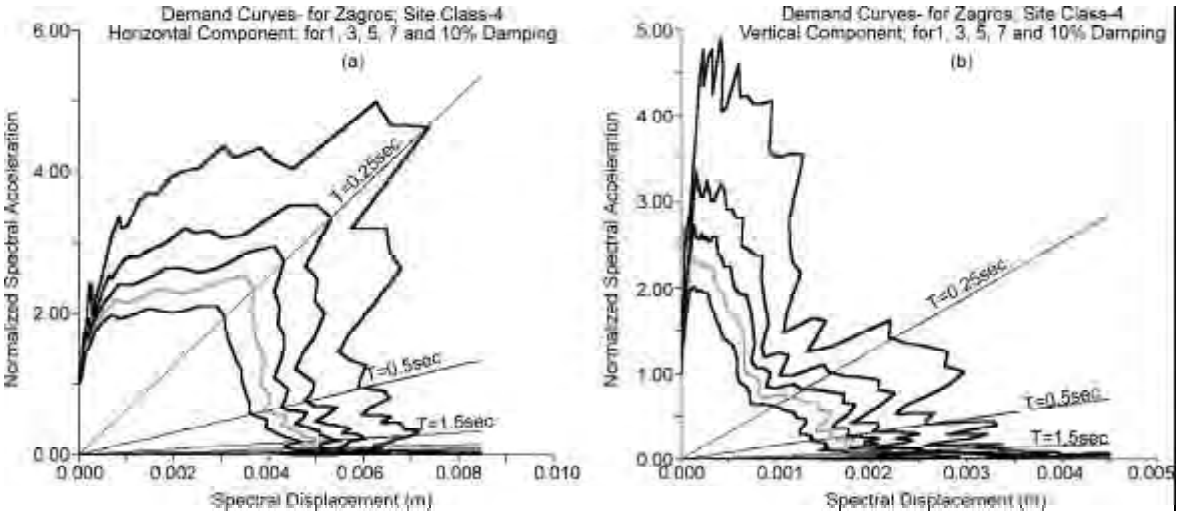

Figure 12. Mean demand curves of Zagros zone, site class-4, for a: horizontal and b: vertical components. The spectral ordinates are represented for different damping of 1, 3, 5, 7, and 10%, and the highest spectrum represent 1% damping and the lower spectra are for 3, 5, 7 and 10% damping, respectively.

3.4. Spectral Displacement for Different Seismotectonic Zones and Site Classes

The mean of the spectral displacement curves is estimated for 1, 3, 5, 7 and 10% of critical damping values. The displacement spectral is not presented in this article, however, such spectrual is presented later only for the near-fault condition.

3.5. Demand Curves and Spectral Displacement for Near-Fault Conditions

Two records of Tabas and Bam with the surface distance to their corresponding surface earthquake fault traces of 1 and 5*km*, are analyzed separately. The site conditions in Tabas is already studied and classified as a seismic bedrock [25]. The site conditions in Bam is studied carefully after Bam earthquake of 26/12/2003, and is of class '3' [26]. The source directivity effects, specially in normal direction faults, were dominant for both of these two records, (in addition to a near vertical directivity for Bam record causing the greatest *PGA* on the vertical component of this record). Therefore, the source effects have been dominant in both cases rather than the site amplification effects (specially in the case of Bam record for which amplification transfer function was evidently different between the mainshock and the aftershocks). Such specific conditions are related to the near-fault conditions for which the mean demand curves are presented in Figure (13) for horizontal and vertical components. The spectral displacement curves for the near-fault conditions are represented in Figure (14) for the horizontal and vertical components.

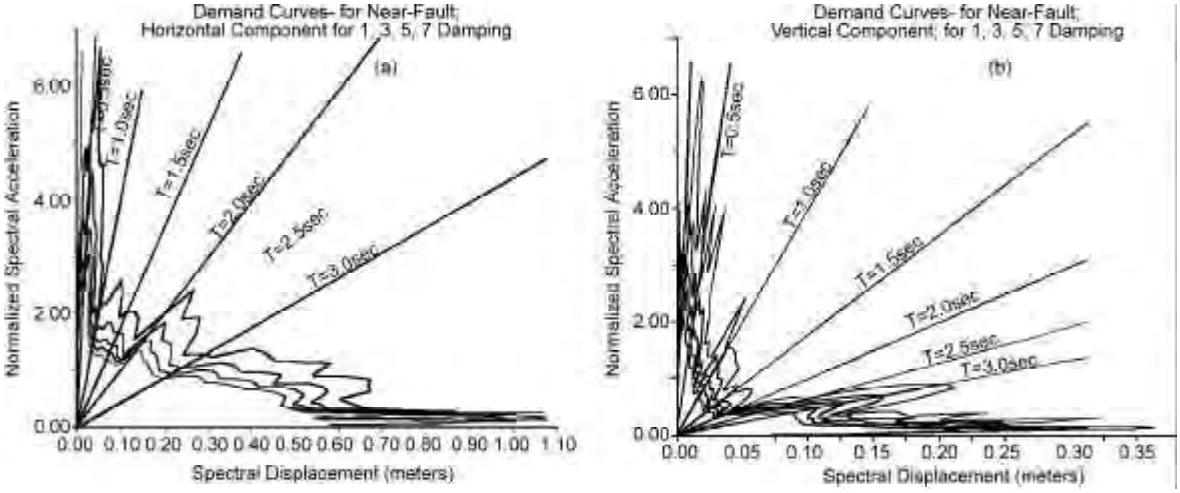

Figure 13. Mean demand curve for the near-fault conditions, for a) horizontal and b) vertical components. The spectral ordinates are represented for different damping of 1, 3, 5, 7, and 10%, and the highest spectrum represent 1% damping and the lower spectra are for 3, 5, 7 and 10% damping, respectively.

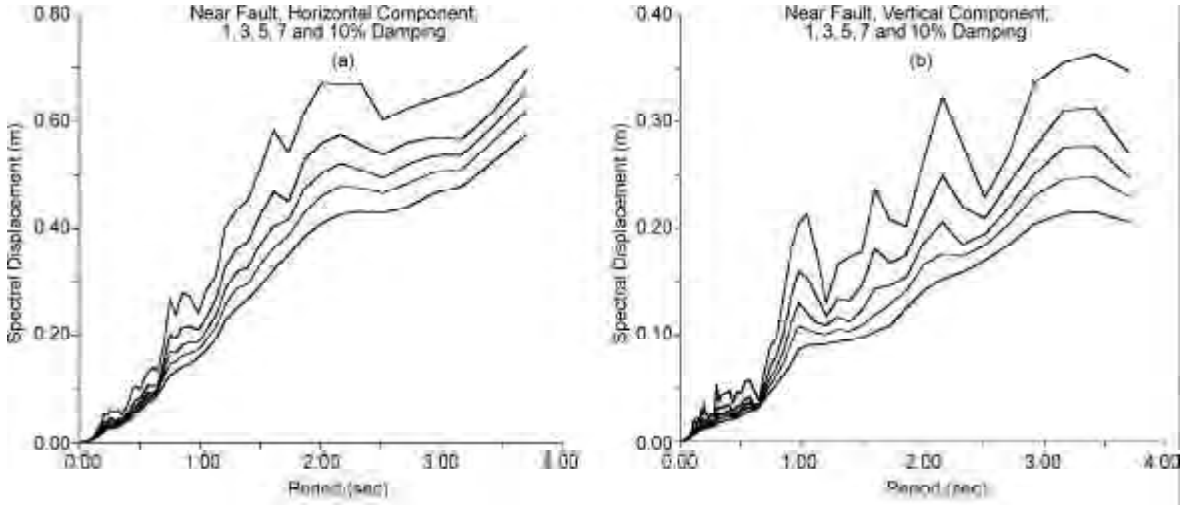

Figure 14. Mean spectral displacement for the near-fault conditions, for a) horizontal and b) vertical components. The spectral ordinates are represented for different damping of 1, 3, 5, 7, and 10%, and the highest spectrum represent 1% damping and the lower spectra are for 3, 5, 7 and 10% damping, respectively.

4. Discussion

The selected records, as shown in Table (1), are presented based on their code (assigned by [9]), station name, site class, band-pass filter selected for each record, *PGA* (for three components), the event's date, coordinates, epicentral region, reported magnitude, focal depths and mechanisms, and the hypocentral distances. The hypocentral distances are estimated for each record based on the *S-P* arrival time method. 89 records corresponding to 45 earthquakes are finally selected.

The selected records have different frequency contents and specifications. These differences are corresponded to the magnitude and hypocentral distances, as well as to the instrument type. Most of the records are noisy in the frequencies less than 0.3*Hz*. However, some digital records show high signal to noise ratios in the frequency band of 0.3*Hz* or lower. The selected records have a *PGA* of equal to or greater than $50 cm/sec^2$ in one component. The discussion on the developed results are summarized as:

- Most of the records are obtained in the distance range of 8 to 100*km*, and in the magnitude range of 4.0 to 7.4, see Figures (3) and (4).
- The demand curves and the spectral displacements have been plotted and compared for two major seismotectonic zones of Alborz-Central Iran and Zagros, and are classified for different site classes. In Alborz-Central Iran region, the means of demand curves for the site class-1 are

representative of spectral acceleration (Sa) for horizontal component greater than the vertical component.

- Alborz-Central Iran has the highest spectral displacement (Sd) in comparison with other site classes, see Figures (13) and (14). However, the mean demand curves of site class-4 in Alborz-Central Iran shows systematic increase in the spectral displacement comparing to those of site classes-2 and 3, see Figure (14).
- The mean demand curves for Zagros region indicate significant difference between site classes 1 and 4 (from the hardest to the softest site conditions). However, based on the existing reliable and selected data for this study, the demand curves and Sd show no significant increase in site classes 2 and 3 in comparison with site class-1, see Figures (13) and (14).
- Considering the demand curves and Sd in Zagros region, spectral displacement and frequency content of the motions are evidently lower comparing to that of Alborz-Central Iran region.
- The near fault demand curves, as shown in Figure (13), show that horizontal component spectra have greater values than that of vertical one caused by the directivity effect which induced long period pulses of SH waves in fault-normal horizontal component of the motion.
- Such difference between the frequency content of the horizontal and vertical components in the near-fault distances is specially evident for spectral displacement ordinates, when the values of horizontal components represent twice the vertical one, see Figure (14).

5. Conclusion

This study was effective to select the higher qualified strong motion records obtained in Iran (1977-2003) with greater amplitudes for studying the spectral demand curves of different seismotectonic zones and 4 site classes. These curves can be used in the rehabilitation and reinforcement projects in Iran and other parts of the world (in the similar seismotectonic and strong motion condition) with the aim of using the damping systems in the important buildings. The mean demand curves, estimated and discussed in this study, showed that the data for site classes 2 and 3 are still insufficient in concluding the systematic changes between different site classes. However, there is significant difference between rock and soft soil sites (1 and 4) in both seismotectonic zones. Therefore, the curves developed in this study is recommended to be used for the site class-1 of the bedrock and then in case of specific site conditions (classes 2, 3 or 4), a "site specific study", geotechnical profiles is used. In order to complete the dataset and receiving homogeneous number of records for different site classes and near-fault conditions, the study should be followed. The author worries about future completeness of the dataset for the near-fault conditions (especially in the case of great earthquakes). In fact, another major catastrophy in Iran similar to Bam earthquake of 26/12/2003, could cause a death toll of more than 33000!.

Acknowledgment

The strong motion data used in this project was released by *BHRC* [9], an organization responsible in maintaining Iranian national strong motion network, for which the author is very grateful. Dr. A. Vasseghi of *IIEES* is really appreciated for his useful suggestions and constructive comments in improving the present study.

References

1. Aki, K. (1967). "Scaling Law of Seismic Spectrum", *J. Geoph. Res.*, **72**, 1217-1231.

2. Askari, F., Azadi, A., Davoodi, M., Ghayamghamian, M.R., Haghshenas, E. Hamzehloo, H., Jafari, M.K., Kamalian, M. Keshavarz, M., Ravanfar, O., Shafiee, A., and Sohrabi-Bidar, A. (2003). "Preliminary Seismic Microzonation of Bam", *Journal of Seismology and Earthquake Engineering, Special Issue on Bam Earthquake*, **5**(4) and **6**(1), 69-80.

3. Bard, P.Y., Zaré, M., and Ghafory-Ashtiany, M. (1998). "The Iranian Accelerometric Data Bank, A Revision and Data Correction", *J. of Seismology and Earthquake Engineering*, **1**(1), 1-22.

4. Boore, D.M. (1986). "Short-Period P and S Wave Radiation from Large Earthquakes: Implications for Spectral Scaling Relations", Bull. Seismol. Soc. of America, **76**(1), 43-64.

5. Boore, D.M., Joyner, W.B., and Fumal, T.E. (1993). "Estimation of Response Spectra and Peak Accelerations from Western North American Earthquakes: An Interim Report", U.S. Geol. Survey, Open-File Report: 93-509, 72p.

6. Boore, D.M., Joyner, W.B., and Fumal, T.E. (1994). "Estimation of Response Spectra and Peak Accelerations from Western North American Earthquakes: An Interim Report", U.S. Geol. Survey, Open-File Report, 94-127, 40p.

7. Brune, J.N. (1970). "Tectonic Stresses and the Spectra of Seismic Shear Waves", *J. Geoph. Res.*, **75**, 4997-5009.

8. Brune, J.N. (1971). "Corrections", *J. Geoph. Res.*, **76,** 5002p.

9. Building and Housing Research Center (BHRC) Website (2004). http://www.bhrc.gov.ir/.

10. Earthquake Research Institute (ERI, University of Tokyo) Website (2004). http://www.eic.eri.u-tokyo.ac.jp/EIC/.

11. FEMA 274, Seismic Rehabilitation Commentary (1997). Website of Building Seismic Safety Council (BSSC), National Institute of Building Sciences, http://www.bssconline.org/.

12. Hanks, T.C. (1982). "B Value and-Seismic Source Models: Implications for Tectonic Stress Variations Along Active Crustal Fault Zones", *J. Geoph. Res.*, **84**, 2235-2242.

13. Hanks, T.C. and Kanamori, H. (1979). "A Moment Magnitude Scale", *J. of Geoph. Res.*, **84**(B5), 2348-2350.

14. Hanson, R.D. and Soong, T.T. (2001). "Seismic Design with Supplementary Energy Dissipation Devices", MNO-8, Earthquake Engineering Research Institute (EERI), Oakland, C.A.

15. Harvard University, Seismology Department Website (2003). http://www.seismology.harvard.edu.

16. Haskell, N.A. (1964). "Total Energy and Energy Spectral Density of Elastic Wave Radiation from Propagating Faults", Bull. Seism. Soc. of America, **54**, 1811-1841.

17. Kennet, B.L.N. and Engdahl, E.L. (1991). "Travel Times for Global Earthquake Location and Phase Identification", *Geoph. J. Int.*, **105**, 429-456.

18. Maggi, A., Priestley , K., and Jackson, J. (2002). "Focal Depths of Moderate and Large Size Earthquakes in Iran", *Journal of Seismology and Earthquake Engineering*, **4**(2-3), - .

19. National Earthquake Information Center (USGS) Website (2004). http://neic.usgs.gov/.

20. NEHRP (2003). "Structures with Damping Systems", Added to Chapter 15 Commentary of FEMA 274, 1997; NEHRP Guidelines for Seismic Rehabilitation of Buildings, Website of the Building Seismic Safety Council (BSSC), National Institute of Building Science; http://www.bssconline.org/.

21. Ramirez, O.M., Constantinou, M.C., Whittaker, A.S., Kircher, C.A., and Chrysostomou, C.Z. (2002). "Elastic and Inelastic Response of Buildings with Damping Systems, *Earthquake Spectra*, **18**(3), 531-547.

22. Theodulidis, N. and Bard, P.Y. (1995). "(H/V) Spectral Ratio and Geological Condition; an Analysis of Strong Motion Data from Greece and Taiwan, (SMART-1)", *Soil Dynamics and Earthquake Engineering*, **14**, 177-197.

23. United States Geological Survey (2001). USGS, Digital Data Series DDS-62-C.

24. Zaré, M. (1999). "Contribution à L'étude Des Mouvements Forts en Iran: du Catalogue Aux Lois D'atténuation", Université Joseph Fourier, Thése de Doctorat (PhD Thesis), 237p.

25. Zaré, M., Bard, P-Y., and Ghafory-Ashtiany, M. (1999). "Site Characterizations for the Iranian Strong Motion Network", *J. of Soil Dynamics and Earthquake Engineering*, **18**(2), 101-121.

26. Zaré, M. (2004). "Bam, Iran Earthquake of 26 December 2003, Mw6.5: A Study on the Strong Ground Motions", *Proceedings of 13th World Conference on Earthquake Engineering, Vancouver*, B.C., Canada, Paper No. 8001.